# AFM, SEM and *in situ* RHEED study of Cu texture evolution on amorphous carbon by oblique angle vapor deposition

F. Tang, C. Gaire, D.-X. Ye, T. Karabacak, T.-M. Lu, and G.-C. Wang
*Department of Physics, Applied Physics and Astronomy, Rensselaer Polytechnic Institute, 110 8th Street, Troy, New York 12180-3590, USA*

(Received 22 November 2004; revised manuscript received 22 April 2005; published 11 July 2005)

The evolution of the crystal orientation of a Cu film grown on an amorphous carbon substrate without intentional heating under $75\pm6°$ oblique angle vapor deposition was investigated *ex-situ* by atomic force microscopy (AFM) and scanning electron microscopy (SEM), and *in-situ* by reflection high-energy electron diffraction (RHEED). At the initial stage of growth ($<\sim12$ nm thick) the diffraction patterns showed uniform rings indicating random nucleations of crystals. With more Cu depositions ($>\sim100$ nm thick) the diffraction pattern started to break symmetrically from the middle of the (111) and (200) rings representing the absence of (111) and (200) planes parallel to the substrate. However, after this transition stage, at the thickness of ~410 nm, the intensity distribution of diffraction patterns appeared asymmetric about the middle of the rings, which is interpreted as the appearance of a tilted (111) texture. Finally the diffraction patterns developed into separated short arcs and showed only a $\langle111\rangle\langle\bar{1}10\rangle$ II-O (two-orientation) texture. By comparing RHEED patterns with the SEM and AFM images of the final film, we argue that the tilted columns having tilted (111) top faces dominate in the later stage of growth. Furthermore, considering the geometry of crystals and shadowing effects, we argue that the vertices of columns having the highest growth velocity normal to the substrate and therefore receiving the maximum flux will dominate the film growth and determine the tilt angle of the texture and the preference of the azimuthal angle orientation.

DOI: 10.1103/PhysRevB.72.035430 PACS number(s): 68.55.Jk, 61.14.Hg, 68.37.Ps, 68.37.Hk

## I. INTRODUCTION

The film morphology and crystal orientation (texture) of a growth front are not only subjects of great interest from a practical point of view but also from fundamental science. Morphology and texture directly control many important physical and chemical properties of the films. Very often film surfaces are created under far-from-equilibrium conditions (limited surface diffusion) so that the morphology is not always smooth and the texture is complex.[1]

A particularly effective way to control the morphology and texture of films is the oblique angle vapor deposition where the flux arrives at the substrate with an angle $\alpha$ with respect to the surface normal.[2–4] This deposition technique has been shown to be capable of producing films having columnar structure with a crystal orientation quite different from that obtained from the normal incidence vapor deposition. The formation of columnar structures in this deposition technique is generally believed to be due to the shadowing effect during growth. The columns tend to tilt towards the direction of the incident flux. For a small incident flux angle $\alpha$, the column tilt angle $\beta$ (with respect to the surface normal) obeys the well-known tangent law, $\tan\beta=\frac{1}{2}\tan\alpha$.[5] For a large incident flux angle, the relation between $\alpha$ and $\beta$ is more consistent with the cosine rule, $\beta=\alpha-\sin^{-1}[(1-\cos\alpha)/2]$, derived by Tait *et al.*[6] based on geometrical considerations.

For oblique angle deposition, the columns are usually single crystal with a crystal orientation direction $\beta'$ (with respect to the surface normal) not equal to the direction of the column tilt angle, $\beta$.[3,7] The prediction of the crystal orientation of columns during oblique angle deposition is not trivial. Recently Paritosh and Srolovitz[7] performed a (1+1)-dimensional simulation of the texture evolution based on a continuum model that included an initial polycrystalline structure randomly nucleated on a surface. They combined a texture selection mechanism proposed by Van der Drift[8] and the shadowing effect to produce their final structures. The crystal orientation selection is a result of the competition among initially randomly nucleated crystals and the final winners are crystals with an orientation that gives the fastest vertical growth direction. This model provides a qualitative account on the phenomena observed in the oblique angle deposition experiments.

In this paper, we present an *in-situ* reflection high-energy electron diffraction (RHEED) study of Cu texture evolution during the oblique angle vapor deposition on an amorphous carbon substrate. We choose amorphous carbon as the substrate because it does not react with Cu during depositions at a temperature $<135\pm15$ °C (with no intentional heating) and can provide an ideal platform to study the evolution of polycrystalline films under the shadowing effect. Diffraction techniques such as x-ray diffraction and RHEED are suitable for the study of texture of thin films. X ray penetrates deep (microns) into the film and the information obtained is an average of the film texture. On the other hand, RHEED is surface sensitive and is an ideal tool to follow the growth front texture evolution in various stages of growth. The results obtained from our RHEED study are therefore complementary to the x-ray diffraction results of final texture of Cu by Alouach and Mankey.[9] In addition, by combining *in-situ* RHEED, *ex-situ* AFM, and SEM analyses in our work, we depict the full three-dimensional structures of the final film in both the real and reciprocal spaces and are able to corre-

 

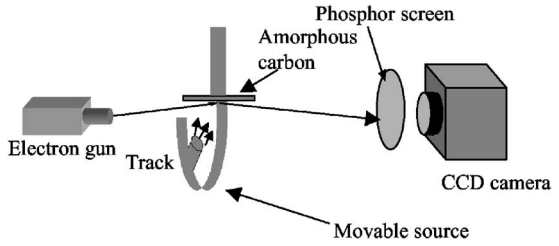


FIG. 1. A schematic of the experimental setup for reflection high-energy electron diffraction and a deposition source. The electron beam is nearly perpendicular to the flux incident plane. The evaporation source is mounted on a semicircle track and the incident beam direction with respect to the substrate can be varied.

late them with each other. Finally, based on the experimental results, two preferred directions of the II-O texture are interpreted as the results of the competition due to the crystal geometry and shadowing effects. We also analytically obtain the relationship between the final texture tilt angle and vapor flux incident angle, using a similar one-dimensional model applied by Paritosh and Srolovitz.[7]

## II. EXPERIMENTS

Conventionally RHEED has been used to monitor molecular beam epitaxy (MBE) during single crystal growth.[10] Recently RHEED has also been shown as a powerful technique to monitor polycrystalline film growth.[11–13] Figure 1 shows a schematic of our experimental growth setup with *in situ* RHEED measurements in an ultra high vacuum chamber. The electron beam is nearly perpendicular to the flux incident plane, which is defined by the direction flux and the substrate normal. The evaporation source can move along a semi-circular track allowing the deposition angles to be varied. Due to the surface roughness of a polycrystalline film, the RHEED displays a three-dimensional (3D) transmission pattern.

AFM (AFM, Auto CP, Park Scientific Instruments) measurements showed that before depositions the substrate had an initial roughness of $\sim$1.2 nm. Our deposition source was made of a Cu foil and a W filament. During a deposition, the Cu foil was heated first by the radiation from the hot W filament and then assisted by electron bombardment from a negatively biased voltage applied to the W filament. More details of the source can be found in Drotar *et al.*'s paper.[13] To reduce the degassing from the surroundings, we first baked out the UHV chamber for $\sim$15 hours at a high temperature. After the chamber was cooled down, the base pressure was $\sim 1\times 10^{-9}$ Torr. Before the first deposition, we degassed the filament of the deposition source. Under radiation only, the pressure was $\sim 2-4\times 10^{-9}$ Torr. Only after we applied the bias between W filament and Cu foil was there a significant release of Cu flux as reflected in the dramatic rise in the measured pressure of $\sim 9\times 10^{-6}$ Torr. This is because the ion gauge was positioned at a small angle (35°) with respect to the surface of the deposition source and lay within the Cu flux. The sample was about 6 cm away from the source. The Cu flux incident angle on the substrate was $75\pm 6°$. The RHEED gun was operated at 10 kV and 0.25 mA emission current. The substrate temperature rose above the room temperature and reached $135\pm 15$ °C within about half an hour due to the irradiation from the source. To avoid possible contaminations on the phosphor screen from the Cu flux, the Cu deposition was interrupted at 11 min ($\sim$12 nm), 90 min ($\sim$100 nm), 6 h ($\sim$410 nm) and 16 h ($\sim 1.1$ $\mu$m) for *in-situ* RHEED measurements. In the experiment the continuous deposition between two interruptions is much longer than to the rising stage of the substrate temperature, so the film basically still grew under the same temperature. To further justify the interrupted measurements, we obtained the RHEED images from the deposited film before turning off the Cu source and also after cooling down of the substrate. We did not find any detectable difference between them. This suggests that the effect of $\sim$100 °C change in the temperature during the temperature rising stage on the crystalline evolution is small. Jian-Min *et al.* also reported that the free-standing Cu films had only a slight enhancement in the (111) texture until an annealing to 300 °C for 2 h.[14] Finally, in the repeated experiment, we observed a similar trend of Cu texture evolution, which did not depend on the interruption of the deposition.

The morphologies and structures of the final Cu films were imaged *ex-situ* by a field emission SEM (FESEM 6330F, Jeol Ltd.) and the AFM. The thickness of the Cu film obtained from the side view of SEM images is $\sim 1.1$ $\mu$m. The thickness refers to the vertical distance between the substrate and the Cu film surface. The growth rate was determined to be $\sim$1.15 nm/min using this thickness divided by 16 h.

## III. RESULTS AND DATA ANALYSIS

### A. SEM and AFM images

Before presenting the *in situ* electron diffraction patterns, we first examine the SEM and AFM images of the Cu film after the completion of depositions. Figures 2(a) and 2(b) show the SEM top view and side view images of the film, respectively. From the top view, we see that isolated tilted columns are formed in the film. Typically these columns have flat planes and are approximately trapezoidally shaped or hexagonally shaped with two elongated sides closely parallel to the flux incident plane (defined by the direction of the incident flux and the surface normal). This regular shape of the column is consistent with its single crystal nature. The top surfaces of columns are tilted away from the substrate normal and the side faces of the columns are closely parallel to each other. This indicates that the crystalline structures possess a preferred azimuthal angle, which will be discussed in detail later in our texture analysis. Besides the columns having trapezoidal or hexagonal shapes, there are also small and compact columns with sharp ends. The SEM side view in Fig. 2(b) shows that the column axes tilt $55\pm 2°$ away from the substrate normal and the columnar structures were formed throughout the entire film.

We also took AFM images of the columns, shown in Fig. 3. AFM images provide quantitative information about the angles of the crystalline planes, which gives us clues to dis-

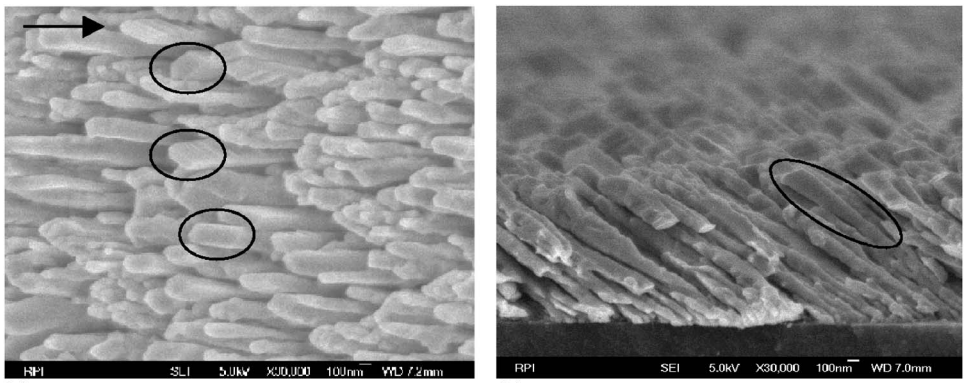


(a) (b)

FIG. 2. The (a) top view and (b) side view of SEM images of the Cu film grown on an amorphous carbon substrate by an oblique angle deposition at ~75° with a total deposition time of 16 h. The scale bars are 100 nm in both (a) and (b). The black arrow in (a) indicates the flux incident direction. The circles mark the typical columns with either trapezoidal or deformed hexagonal shapes. The axes of column structures in (b) tilt about 56° away from the substrate normal. The vertical thickness is ~1.1 $\mu$m. The circled column shows an obvious increase of the column width during growth.

tinguish the planes when the information is combined with the texture analysis to be discussed later. To determine the orientation of the top surfaces, for example, face *A*, we selected three points marked on face *A*. The distances between points we selected in the face are from ~50 to ~150 nm. Since the typical radius of AFM tip is ~10 nm, the effects of AFM radius on the coordinates of points during the calculation could be ignored. Through the image processing software, we can obtain the spatial coordinates of these three points and calculate the geometrical directions of the corresponding faces. We found that the top surface of the column is tilted 33±7° away from the substrate normal. In a similar way we can calculate the geometrical direction of the side face *B* (parallel to the flux incident plane) of the column by choosing three points on face *B*. We measured the angle between faces *A* and *B* to be 100±6°. The angle between the top face and the face *C* perpendicular to the flux incident plane is found to be 120±8°. Another angle of interest is the angle between faces *B* and *C*, which is 59±6°. Considering the AFM tip effects (finite size and instrument convolution),[1] these angles may be overestimated due to the steep drop along the side faces of the columns.

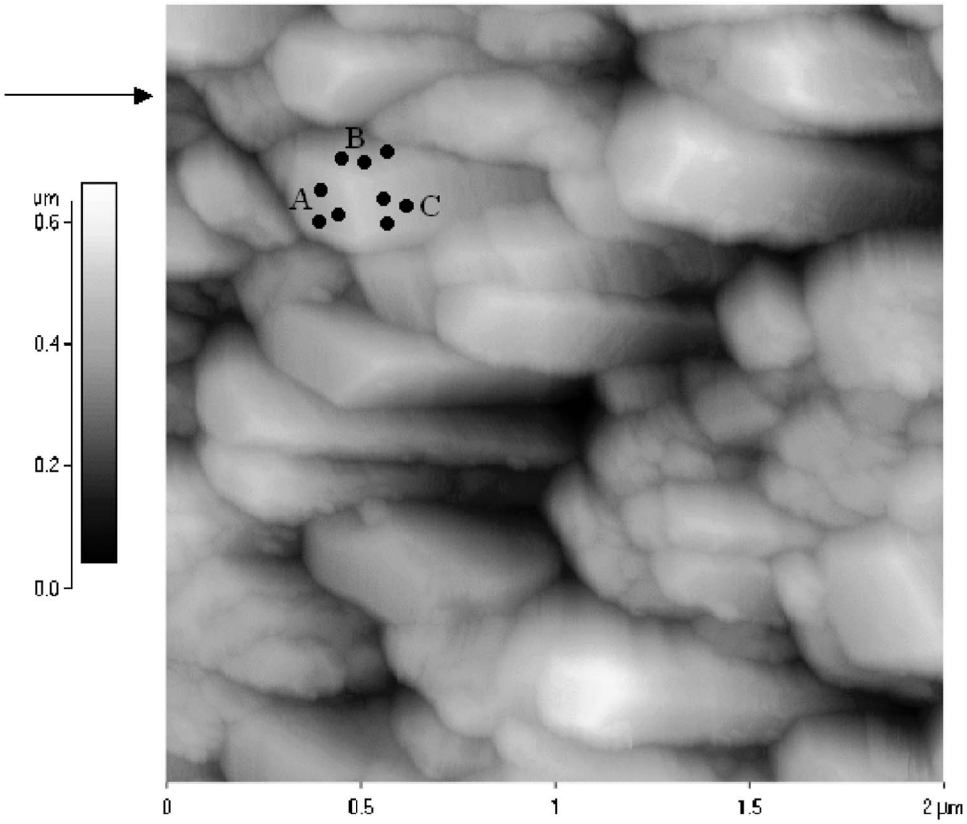


FIG. 3. A $2\times2$ $\mu m^2$ AFM image of the Cu film grown on an amorphous carbon substrate by an oblique angle deposition at ~75° with a total deposition time of 16 h. The black arrow indicats the Cu flux incident direction. Three points used for determining the corresponding geometry directions are marked each on the top face *A*, the side face *B* closely parallel to the Cu flux, and the side face *C* perpendicular to the Cu flux.

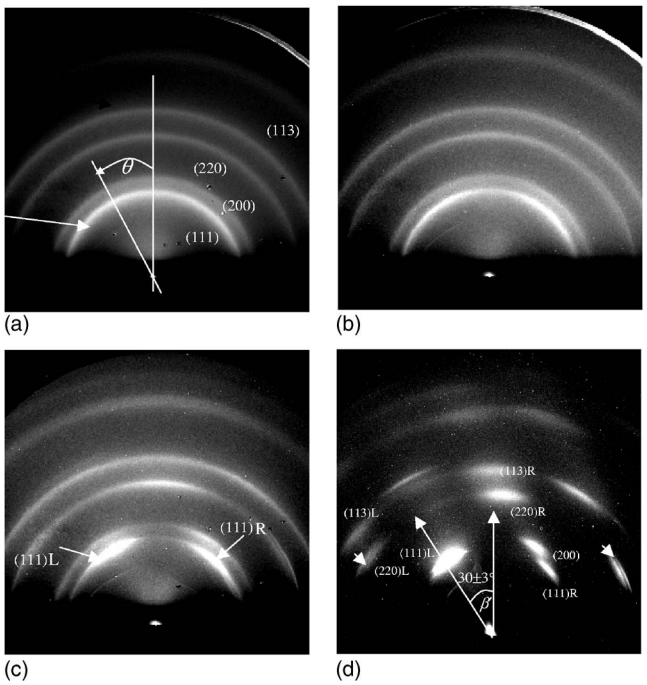


FIG. 4. The RHEED patterns of the Cu film grown on an amorphous carbon substrate by an oblique angle deposition at ~75° for (a) 11 min (b) 91 min, (c) 6 h, and (d) 16 h. The (111), (200), (220), and (113) diffraction rings are labeled in (a). The white arrow on the same pattern (a) represents the flux incident direction. $\theta$ is the polar angle measured from the vertical line in the middle. The two short white arrows in pattern (d) point to the splittings in the (220) diffraction arcs. $\beta$, is the tilt angle of the texture. All the images were taken with the electron beam direction nearly perpendicular to the flux incidence plane.

### B. RHEED patterns and texture analysis

Figures 4(a)–4(d) show the RHEED images of Cu crystalline evolution obtained with the electron beam direction perpendicular to the flux incident plane. From Fig. 4(a), continuous and uniform diffraction rings appeared at the very initial stage of growth. These rings indicate a random nucleation of Cu crystals (with all possible orientations) on the amorphous C substrate. The ratio of the square of the radii of rings from the inner to the outer rings is $3:3.93:8.1:11.2 \approx 3:4:8:11$. The lattice constant measured from the diffraction pattern is $3.63 \pm 0.18$ Å. Both values are consistent with a face centered cubic (fcc) crystal structure of Cu. The relatively large error in the measured lattice constant is due to the uncertainty in the measured distance between the sample and the phosphor screen.

#### *1. Development of tilted (111) texture*

With more depositions, the (111) and (200) diffraction rings started to symmetrically break in the middle as shown in Fig. 4(b), although the flux was incident from a large oblique angle that breaks the symmetry. This breaking means that the (111) and (200) crystal planes normal to the substrate started disappearing and represents the development of the weak textures normal to the substrate surface. However, since there are no other obvious breaks in the higher order

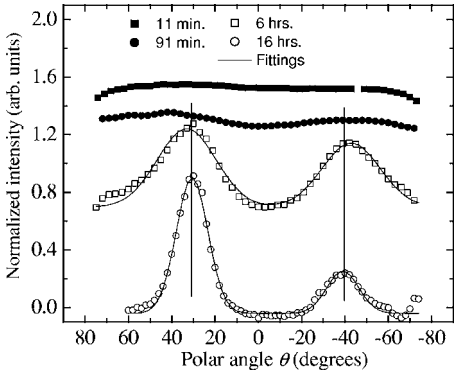


FIG. 5. The normalized intensity of the (111) rings versus polar angle $\theta$ for the RHEED patterns measured at 11 min, 91 min, 6 h, and 16 h Cu depositions on amorphous carbon substrate at an oblique angle ~75°.

diffraction rings such as the (220), (113), etc., the film is composed of several weak textures like the (220), (113), etc. In Fig. 4(c), the middle of the (111) and (200) rings broke further, and the distribution of positions of arcs were still approximately symmetrical about the substrate normal, which indicates that there still exists preferred orientations normal to the substrate. However, the intensity of the arc on the left that we labeled (111)L is higher than the intensity of the arc (111)R. This asymmetry in intensity indicates a tilted (111) texture determined from Fig. 4(d). In Fig. 4(d), clear and asymmetrically distributed arcs are shown. These arcs represent well-developed textures. From Fig. 4(d) we can see an extremely strong intensity (111)L arc rotating $30 \pm 3°$ away from the central vertical axis of the image. This indicates that the crystals having a preferred (111) direction are tilted about 30° away from the normal of the substrate. In addition we observe symmetric distributions of (220)L, (220)R, (113)L, and (113)R arcs at angles of ±35° and ±29°, respectively, with respect to the brightest (111)L arcs. Therefore this pattern suggests that the final film has a tilted (111) texture. One character of the tilted (111) texture is the much stronger intensity of arc (111)L than arc (111)R.

In addition to the development of broken rings and unsymmetrical intensity in the RHEED pattern, we observed two sharp (220) arcs close to the shadow edge (the horizontal boundary separating the nonzero intensity and zero intensity parts near the bottom of each figure) also appeared and formed fine splittings as shown in Fig. 4(b), and became more clear in Figs. 4(c) and 4(d). These splittings in the diffraction may be due to the refraction of electrons from the facets of crystals having regular shapes, which are seen in our SEM images. Using the method illustrated by Cowley and Rees,[15] we calculated the splittings of the (220) diffraction arcs near the shadow edge due to the refraction effect to be ~2.1% of the radius of the (220) diffraction ring. This value is close to our experimentally determined value of ~2.5% measured from the RHEED patterns.

To obtain more quantitative information about the crystal orientation, in Fig. 5 we present the normalized intensities of the (111) ring at various times versus the polar angle ($\theta$). The polar angle is defined as the angle measured from the vertical axis perpendicular to the substrate as shown in Fig. 4(a). The

process of the intensity normalization was described in detail in Drotar *et al.*'s work.[13] In short, we first subtracted the background intensity from the intensity of the (111) ring. Next, the intensity, after removing the background, was divided by the background intensity. From the figure we can see that with more depositions the initial flat intensity at 11 min developed into a curve having two peaks, corresponding to the (111)L and (111)R arcs, at polar angles of ~30° and ~−40°, respectively. The polar angle between these two peaks is ~70°, which is the angle between the ⟨111⟩ and ⟨11$\bar{1}$⟩ directions. For the 91 min deposition, the pattern has an intensity decrease in the middle and the curve shows two weak but nearly symmetrical peaks. At the 6 h deposition, the intensity of the peak at 30° is higher than the intensity of the peak at −40°. For the final film formed after the 16 h deposition, the peak at 30° is very strong and prominent, which is characteristic of a well-developed tilted (111) texture. We fit the individual curves for longer depositions with two Gaussian peaks. For early deposition data (11 and 91 min), the peaks are too weak to be fit. For the 6 h deposition, the intensity ratio between fitted peaks at ~30° and ~−40° and the FWHM of peak at ~30° are 1.25±0.03 and 31.7±0.4°, respectively. For the final 16 h deposited film, these values are 3.20±0.03 and 16.5±0.2°. Judging from these data, we can say that there is an obvious development of the (111) texture between 6 and 16 h. Further, when the electron beam is perpendicular to the texture axis, the intensity of the diffraction peak of a tilted ⟨111⟩ fiber texture is approximately proportional to $p/\Delta\theta$,[16] where $p$ is a multiplicity factor and $\Delta\theta$ is a dispersion angle. For the ⟨111⟩ directions, $p$ is 1 and the FWHM of the peak $\Delta\theta$ is 16.5°; for the ⟨11$\bar{1}$⟩ directions $p$ is 3 and $\Delta\theta$ is 360°, since the tilted ⟨111⟩ fiber texture has randomly distributed azimuthal angle orientations, which are defined around the ⟨111⟩ direction. So for a tilted ⟨111⟩ fiber texture the $p/\Delta\theta$ ratio between peaks at ~30° and ~−40°, corresponding to ⟨111⟩ and ⟨11$\bar{1}$⟩ directions, is ~7.3(=(1/16.5)/(3/360)). Comparing with the value of 7.3, the lower ratio of 3.2 measured from the intensity from the final film indicates a limitation of the azimuthal angle orientation.

#### *2. Preferred azimuthal angle orientation*

From the AFM images, we obtained that the top surface of a column is tilted ~30° away from the normal of the substrate. This face is the (111) crystalline plane consistent with the diffraction patterns. A closer look at the SEM images also indicates that the side faces of the columns are almost parallel to each other. Thus the crystals should have an azimuthal angle selection during the formation of the columns. Considering the (111) plane of an fcc structure, the lines having ⟨$\bar{1}$10⟩ directions have the closest adjacent atoms. These atomic rows give the edges of hexagonal or trapezoidal islands, which were reported in previous field ion microscopy works.[17] So we argue that the edges of the columns closely parallel to the flux incident direction represent a preferred ⟨$\bar{1}$10⟩ direction. Below we will simulate the diffraction pattern of (111)⟨$\bar{1}$10⟩ (II-O) texture, in which both preferred crystal axes lie in the flux incident plane.[18] We find this texture does give a consistent picture with the experimental diffraction patterns.

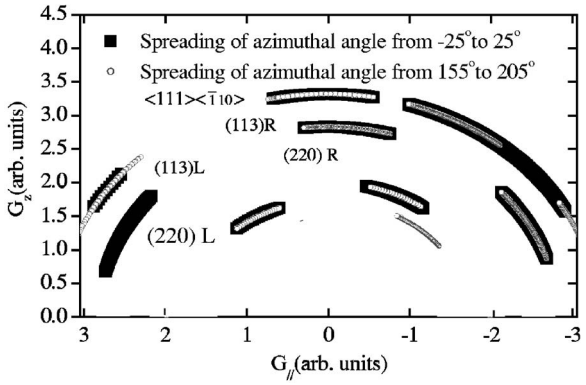


FIG. 6. The calculated diffraction patterns for the ⟨111⟩⟨$\bar{1}$10⟩ II-O texture. $G_{\|}$ and $G_z$ represent the parallel and normal components of the reciprocal lattice vector G, respectively.

Litvinov *et al.*[11] showed an analytical solution for the diffraction pattern of a fiber texture that has no preferred azimuthal orientation. However, for the diffraction with preferred azimuthal orientations, there is no analytical solution and the explanation of diffraction patterns is not a straightforward matter. Figure 6 shows our computed diffraction pattern of a texture having a ⟨111⟩ preferred direction tilted 30° away from the substrate normal and a ($\bar{1}$10) preferred direction with azimuthal angles $\phi \sim 0°$ and ~180°. The spreading angles of the calculated arcs (10°) representing the range of the crystalline orientation is chosen to fit the experimental (220)R arc. The (111) arc is broader due to the splitting. 0° is defined as the direction when the ⟨$\bar{1}$10⟩ is in the flux incident plane. If we look at the partial hexagon structure in Fig. 2(a), 180° rotation around the ⟨111⟩ axis will give a symmetrical shape. So the columns with ~180° azimuthal angle rotation are also included in the diffraction pattern. Since the ⟨111⟩ direction is a threefold symmetry axis, this 180° rotation will give a different crystal orientation with a different diffraction pattern. From the simulated pattern shown in Fig. 6 we can see that (220)L, (220)R, (113)L, and (113)R are symmetrically distributed around the (111)L arc. This simulated pattern is consistent with the RHEED pattern we obtained in Fig. 4(d). In the calculation the electron beam is assumed to be 10° away from the direction perpendicular to the flux incident plane. This 10° deviation is closer to our experimental condition in which the electron beam was nearly perpendicular to the flux incident plane. The dispersion of the (111) texture axis is assumed to evenly spread in the directions parallel and perpendicular to the flux incident plane. In order to obtain the symmetrically distributed arc patterns, an azimuthal angle dispersion has to be assumed to be at least 25°. We only calculated the arcs associated with indices of crystalline planes up to (113) which have the strong intensity observed in the experimental patterns.

## IV. DISCUSSION

At the initial stage, the crystallines developed from random orientations to the absence of (111) and (200) crystal-

line orientations parallel to the substrate and indicated weak textures normal to the substrate. This evolution may be due to different atomic mobilities on different crystalline planes, which are illustrated in Drotar *et al.*'s work.[13] For the grains having higher index crystalline planes parallel to the substrate, the atomic mobility is lower and therefore they have higher vertical growth rate. Since the starting substrate is very smooth with a roughness of ~1.2 nm, in the initial growth stage the diffusion of Cu atoms can overcome the roughness and the effects of the flux at an oblique incident angle. In this case, the Cu film was dense and tilted columns will not be expected. This could account for the development of weak textures normal to the substrate in the beginning of growth. However, with more depositions, the tilted (111) texture started to appear and gradually dominated the film.

To understand the development of the tilted (111) texture, we first go back to examine the SEM images in Fig. 2. From the cross-sectional view, we can see that the film started with very small and compact columns. The columns having slanted flat top faces grew much bigger in size at the later stage. The circled column shows the most obvious width increase during the growth. From the above analysis, we know that these large columns have the (111) planes facing the flux. Besides these large columns, there also exist small columns with sharp ends, which are clearly seen in the top view of SEM images. We argue that the small columns have top faces, which are not (111) planes. These columns almost do not show any increase of the column width. The much higher lateral growth of the columns having the (111) planes towards the deposition flux is ascribed to the much higher adatom mobility on the (111) planes. With the rising substrate temperature due to the radiation, the increase of the column width will even be speeded up. Since the (111) plane is tilted away from the substrate normal, the expansion of the top face will also cause the vertical growth of the columns, which shadows the adjacent columns.[18,19] As a result of the growth, the columns having the (111) planes as the top surface will dominate the film. This column competing growth process is consistent with a gradual development of the tilted (111) texture.

### A. Tilted (111) texture

The columns having the (111) planes towards the deposition flux also show a preferred tilt angle of ~30° from the substrate normal. The inset of Fig. 7(a) shows a schematic of one column. From the figure we can see that the column width gradually increases. The top face is the (111) plane with $\langle \bar{1}10 \rangle$ directions parallel to the edges. The top (111) plane tilts away from the substrate normal at an angle of $\beta'$, which is different from the column tilting angle $\beta$. We argue that this preferred tilting angle $\beta'$ is related to the faster growth of the columns whose vertices (the intersection between different faces) grow the highest in the direction normal to the substrate under the oblique angle deposition. Due to the shadowing effects, these columns will obtain more flux and finally win.

We now show the detailed calculation of the tilt angle of the texture based on a similar one-dimensional model used

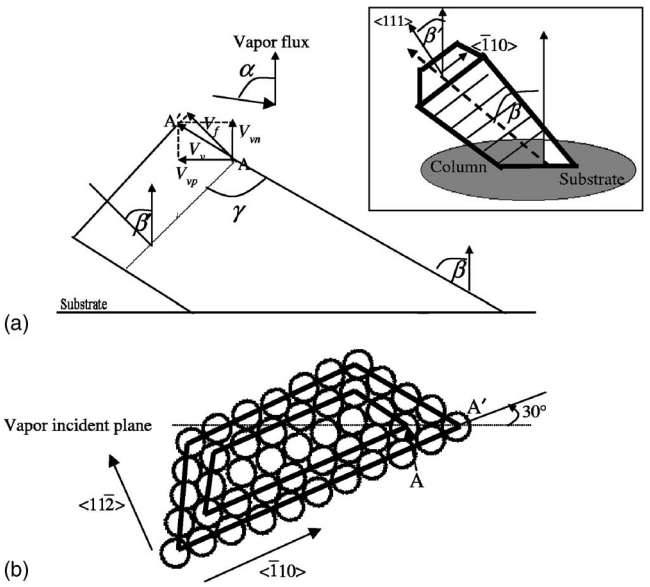


FIG. 7. (a) A schematic of the growth of one column along the column axis. $\beta$ and $\beta'$ are the tilt angles of the top face and column axis measured from the substrate normal, respectively. $\alpha$ is the flux incident angle and $\gamma$ is the angle between two faces. $V_f$ is the velocity perpendicular to the top face. The growth velocity $V_v$ of vertex $A$ is projected to components $V_{vp}$ and $V_{vn}$ that are parallel and normal to the substrate, respectively. The inset shows a 3-D schematic of a column. (b) A schematic of the growth of the top surface of one column viewed perpendicular to the (111) plane, in which $\langle \bar{1}10 \rangle$ aligns at $\phi \sim 30°$ with respect to flux incident plane. The dashed line represents the flux incident plane viewing perpendicular to the (111) plane. The small inner trapezoid bordered by gray lines and the larger outer trapezoid bordered by dark lines are the top faces of the column at the two consequent growth times. Each open circle represents an atom. The $\langle \bar{1}10 \rangle$ and $\langle 11\bar{2} \rangle$ directions are perpendicular to the $\langle 111 \rangle$ direction.

by Paritosh and Srolovitz in their simulation.[7] Using this model we consider the growth along the column axis and neglect the increase of column width shown in the inset of Fig. 7(a). Let $\gamma$ be the angle between two faces as shown in Fig. 7(a). The growth velocity $V$ of a facet is given by[7]

$$V = \hat{n} \cdot \vec{J}, \tag{1}$$

where $\hat{n}$ is the facet normal and $\vec{J}$ is the flux. Then the growth velocity of the facet toward the flux incident direction in Fig. 7(a) is

$$V_f = J \cos(\alpha - \beta'). \tag{2}$$

The velocity of a vertex $V_v$ is

$$V_v = \frac{V_f}{\sin \gamma} = \frac{J \cos(\alpha - \beta')}{\sin \gamma}. \tag{3}$$

$V_v$ can be divided into components $V_{vp}$ and $V_{vn}$ that are parallel and normal to the substrate, respectively. From the geometry shown in Fig. 7, we can obtain the velocity of the vertex normal to the substrate as

$$V_{vn} = \frac{J\cos(\alpha - \beta')\sin(\beta' + \gamma)}{\sin\gamma}. \quad (4)$$

It has a maximum velocity when

$$\beta' = 45^\circ + (\alpha - \gamma)/2. \quad (5)$$

From the AFM image, $\gamma$ was found experimentally to be $120 \pm 8^\circ$. This value is close to the angles between the (111) and $(\bar{1}\bar{1}1)$ or $(\bar{1}00)$ planes, which are 109.5° and 125°, respectively. These two planes are the two side facets of the (111) columns. Substituting our measured $\gamma$ value of 120° and $\alpha$ of 75°, the predicted value of $\beta'$ is 22.5°. In the one-dimensional model, there is a relation of

$$\beta' = 90^\circ + \beta - \gamma. \quad (6)$$

Combining Eqs. (5) and (6) we can obtain

$$\beta = \alpha - \beta'. \quad (7)$$

So the predicted $\beta$ is 52.5°. Both these values of $\beta'$ and $\beta$ are smaller than the corresponding experimental values of ~30° and ~55°, respectively. Possible reasons for this may be the limitation of the one-dimensional model and a large uncertainty of the flux incident angle.

### B. Preferred azimuthal angle orientation

Although the above one-dimensional model gives a qualitative prediction of the tilt angle, it cannot give any information on the azimuthal angle selection of the columns observed in the experiment. A number of arguments have been presented in the literature to explain the azimuthal angle selection.[18,20,21] Here we present a simple way to account for this effect in our oblique angle deposition of Cu. Due to the tilt of the top faces, when the elongated sides of the crystals are approximately parallel to the flux incident plane, the crystals will obtain the highest vertical growth rates. Figure 7(b) shows a schematic of the growth of the top surface of one column viewing perpendicularly to the top (111) plane. The surface is enclosed by close packed edges having $\langle \bar{1}10 \rangle$ directions. The corresponding column was circled in the top view of SEM image [Fig. 2(a)]. In this case we consider the increase of the column width. After a certain amount of deposition, the inner trapezoid bordered by gray lines expands to a larger trapezoid bordered by dark lines and the tip $A$ of the column grows to $A'$. We can see that the tip has the fastest growth rate. Since the top face is tilted away from the normal of the substrate, this increase of column width will cause the vertical growth of the column at the same time. Provided that the $\langle \bar{1}10 \rangle$ direction makes an angle of 30° with respect to the flux incident plane, the tip will also have the fastest vertical growth and the corresponding column will finally survive. Considering the equivalence of the edges and the change of symmetry of a partial hexagon, the $\langle \bar{1}10 \rangle$ axis will be dispersed within $\sim \pm 30^\circ$ and $180 \pm 30^\circ$, which is consistent with our RHEED analysis.

## V. CONCLUSION

In this paper, we studied the texture evolution of Cu columnar structures on an amorphous carbon substrate grown by the oblique angle (~75°) vapor deposition technique using *in situ* RHEED, *ex situ* AFM, and SEM. The development of the $\langle 111 \rangle \langle \bar{1}10 \rangle$ texture, from randomly oriented Cu crystals and through an intermittent stage having textures normal to the substrate, was measured as a function of time. In the final stage, the $\langle 111 \rangle$ texture was found to tilt $30 \pm 3^\circ$ away from the substrate normal but the $\langle \bar{1}10 \rangle$ direction was confined within 30° with respect to the flux incident plane. By comparing RHEED patterns with the SEM and AFM images of the final film, the crystalline evolution is correlated to the development of a columnar structure with a trapezoidal crystal shape at the top surface. Considering the geometry of crystals and shadowing effects, we argue that the vertices of columns having the highest growth velocity normal to the substrate and therefore receiving the maximum flux will dominate the film growth and determine the tilt angle of the texture and the preference of the azimuthal angle orientation.

## ACKNOWLEDGMENTS

This work was supported in part by the NSF. We thank Dr. H. Huang for valuable discussions.

[1] Y.-P. Zhao, G.-C. Wang, and T.-M. Lu, *Characterization of Amorphous and Crystalline Rough Surface—Principles and Applications* (Academic Press, New York, 2001).
[2] K. Robbie and M. J. Brett, J. Vac. Sci. Technol. A **15**, 1460 (1997).
[3] Leon Abelmann and Cock Lodder, Thin Solid Films **305**, 1 (1997).
[4] Y.-P. Zhao, D.-X. Ye, G.-C. Wang, and T.-M. Lu, Proc. SPIE **5219**, 59 (2003).
[5] A. G. Dirks and H. J. Leamy, Thin Solid Films **47**, 219 (1997).
[6] R. N. Tait, T. Smy, and M. J. Brett, Thin Solid Films **226**, 196 (1993).
[7] F. Paritosh and D. J. Srolovitz, J. Appl. Phys. **91**, 1963 (2002).
[8] A. van der Drift, Philips Res. Rep. **22**, 267 (1967).
[9] H. Alouach and G. J. Mankey, J. Vac. Sci. Technol. A **22**, 1379 (2004).
[10] J. I. Harris, B. A. Joyce, and P. J. Dobson, Surf. Sci. **103**, L90 (1981).
[11] Dmitri Litvinov, Thomas O'Donnell, and Roy Clarke, J. Appl. Phys. **85**, 2151 (1999).
[12] Stéphane Andrieu and Patrick Fréchard, Surf. Sci. **360**, 289 (1996).
[13] Jason. T. Drotar, T.-M. Lu, and G.-C. Wang, J. Appl. Phys. **96**, 7071 (2004).
[14] Jia-Min Zhang, Ke-Wei Xu, and Vincent Ji, Appl. Surf. Sci. **187**, 60 (2002).

[15] J. M. Cowley and A. L. G. Rees, Proc. Phys. Soc. London **59**, 287 (1947).
[16] B. K. Vainshtein, *Structure Analysis by Electron Diffraction* (The Macmillan Company, New York, 1947).
[17] S. Liu, Z. Zhang, G. Comsa and H. Metiu, Phys. Rev. Lett. **71**, 2967 (1993).
[18] E. Bauer, *Ninth Nat. Vacuum Symp. Am. Vac. Soc.*, edited by George H. Bancroft (Macmillan, New York, 1963).
[19] Hanchen Huang and G. H. Gilmer, J. Comput.-Aided Mater. Des. **6**, 117 (1999).
[20] Katsuya Hasegawa, Yuichi Nakamura, Teruo Izumi, and Yuh Sohiohara, Physica C **357–360**, 967 (2000).
[21] O. P. Karpenko, J. C. Bilello, and S. M. Yalisove, J. Appl. Phys. **82**, 1397 (1997).